

# Polyhedral metallaheteroborane chemistry. Synthesis, spectroscopy, structure and dynamics of eleven-vertex $\{\text{RhNB}_9\}$ and $\{\text{PtCB}_9\}$ metallaheteroboranes.†

Ramón Macías,<sup>\*a,b</sup> Jonathan Bould,<sup>a</sup> Josef Holub,<sup>a,c</sup> John D. Kennedy,<sup>a</sup> Bohumil Štíbr<sup>c</sup> and Mark Thornton-Pett<sup>a</sup>

Received 22nd February 2007, Accepted 23rd March 2007

First published as an Advance Article on the web 1st May 2007

DOI: 10.1039/b702767b

Reaction between  $[\text{RhCl}(\text{PPh}_3)_3]$  and the  $[\text{nido-6-NB}_9\text{H}_{11}]^-$  anion in  $\text{CH}_2\text{Cl}_2$  yields orange eleven-vertex  $[\text{8,8-(PPh}_3)_2\text{-nido-8,7-RhNB}_9\text{H}_{11}]$  (**1**). Reaction of the  $[\text{nido-6-CB}_9\text{H}_{12}]^-$  anion with  $[\text{cis-PtCl}_2(\text{PMe}_2\text{Ph})_2]$  in methanol affords yellow eleven-vertex  $[\text{9-(OMe)-8,8-(PMe}_2\text{Ph)}_2\text{-nido-8,7-PtCB}_9\text{H}_{10}]$  (**2**), which is also formed from the reaction of MeOH with  $[\text{8,8-(PPh}_3)_2\text{-nido-8,7-PtCB}_9\text{H}_{10}]$  (**3**). Both compounds have been characterised by single-crystal X-ray diffraction analysis and examined by NMR spectroscopy and have structures based on eleven-vertex *nido*-type geometries, with the metal centre and the heteroatoms in the adjacent (8)- and (7)-positions on the pentagonal open face. The metal-to-heteroborane bonding sphere of **1** is fluxional, with a  $\Delta G^\ddagger$  value of  $48.4 \text{ kJ mol}^{-1}$ . DFT calculations on the model compounds  $[\text{8,8-(PH}_3)_2\text{-nido-8,7-RhNB}_9\text{H}_{11}]$  (**1a**) and  $[\text{8,8-(PH}_3)_2\text{-nido-8,7-RhSB}_9\text{H}_{10}]$  (**4a**) have been carried out to define the fluxional process and the intermediates involved.

## Introduction

In 1990 the eleven-vertex rhodathiaborane,  $[\text{8,8-(PPh}_3)_2\text{-nido-7,8-RhSB}_9\text{H}_{10}]$  **4** was reported.<sup>1</sup> This compound exhibits a fluxional behaviour in solution, which was described as the transfer of the  $\{\text{Rh}(\text{PPh}_3)_2\}$  unit from one side to the other of the *nido*-shaped ten-vertex  $\{\text{SB}_9\text{H}_{10}\}$  fragment. Subsequently, the isoelectronic platinacarborane,  $[\text{8,8-(PMe}_2\text{Ph)}_2\text{-nido-8,7-PtCB}_9\text{H}_{11}]$  **3**, was also described.<sup>2</sup> Compound **3** also exhibits dynamic behaviour related to that of the rhodathiaborane, but, for this species, the presence of the phosphine  $\text{PMe}_2\text{Ph}$  generated prochiral centres that allowed a more complete characterization of the fluxional process. This process was described as a shift of the platinum atom across the open face of the  $\{\text{CB}_9\text{H}_{10}\}$  cluster, linked with a half-rotation of the  $\{\text{PMe}_2\text{Ph}\}_2$  ligand sphere.

These two eleven-vertex metallaheteroboranes are examples of borane-based clusters that contain square-planar sixteen-electron transition-element centres, and which could be taken to appear to deviate from the classical Wade–Williams cluster-geometry electron-counting relationship.<sup>3</sup> According to a common interpretation of this relationship, the structural architecture, geometrically classed as *nido*, would formally require 13 skeletal electron pairs (sep) to attain a *nido* structure. However, an electron count of the constituent vertices gives only 12 sep for either

cluster. The clusters could therefore perhaps be regarded as being formally unsaturated, albeit with the unsaturation localised on the sixteen-electron metal centre. This unsaturation implies enhanced reactivity, and, in accord with this, the rhodathiaborane cluster can add a Lewis base without change of the *nido* geometry, it can undergo facile substitution of the  $\text{PPh}_3$  ligands, and it can undergo a *nido* to *closo* transformation, as well as exhibiting other interesting reactivity.<sup>1,4</sup>

The nature of the apparent electronic disobedience of these metallathiaboranes has been recently reviewed in *Comprehensive Organometallic Chemistry*, third edition (COMC-III),<sup>5</sup> where it is pointed out that  $[\text{8,8-(PPh}_3)_2\text{-nido-7,8-RhSB}_9\text{H}_{10}]$  **4** and  $[\text{8,8-(dppe)-nido-7,8-RhSB}_9\text{H}_{10}]$  **5**,<sup>6</sup> were proposed to exhibit two ‘agostic’ *ortho*-CH-to-Rh interactions that endow the metal centre with extra electrons, and hence furnish the overall cluster with the extra electron pair required to agree with Wade’s electron counting rules.<sup>3</sup> However, it is not clear how two such interactions, involving a total of four electrons, should be necessary to provide only two extra cluster electrons. As an alternative rationale, it has been pointed out,<sup>7</sup> though not so reviewed in COMC-III, that there is no need to invoke such agostic interaction if the transition-element centres concerned are comfortable with a sixteen-electron configuration. An interpretative problem often arises because simplistic applications of electron-counting rules often presume eighteen-electron transition-element behaviour.

The principal synthetic route to  $\text{MEB}_{10}$ -types of metallaheteroboranes (where E is C, N or S, and M is a transition-element centre) has been that of metal-centre insertion into the open face of the carbaborane precursor  $[\text{arachno-6-CB}_9\text{H}_{14}]^-$ ,<sup>8</sup> the isoelectronic thiaborane  $[\text{arachno-6-SB}_9\text{H}_{12}]^-$ ,<sup>9</sup> and the azaborane precursors  $[\text{arachno-6-NB}_9\text{H}_{13}]^-$  and *nido-6-NB}\_9\text{H}\_{12}.<sup>10</sup> However, stable heteroborane substrates are often not robust and their preparation is often complicated. These two factors have inhibited*

<sup>a</sup>School of Chemistry, University of Leeds, Leeds, UK LS2 9JT

<sup>b</sup>Instituto Universitario de Catálisis Homogénea, Universidad de Zaragoza, Pedro Cerbuna 12, 50009, Zaragoza, Spain. E-mail: rmacias@unizar.es

<sup>c</sup>Institute of Inorganic Chemistry, The Academy of Sciences of the Czech Republic, 24068, Rez near Prague, The Czech Republic

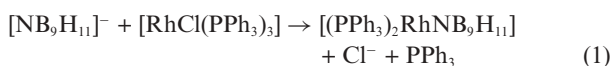
† Electronic supplementary information (ESI) available: X-ray diffraction details, atomic coordinates, bond lengths and angles, isotropic and anisotropic displacement parameters. DFT calculated coordinates for **1a**, **4b** (ground and transition states). See DOI: 10.1039/b702767b

an extensive development of the corresponding metallated cluster chemistry. This is particularly manifest in the metallazaborane area, which, compared to metallamonocarboranes and metallathaboranes, is sparsely examined. We have now found that a convenient approach to eleven-vertex azametallaborane chemistry can derive from the use of the salt [tmndH][NB<sub>9</sub>H<sub>11</sub>] (where tmnd is *N,N,N',N'*-tetramethylnaphthalene-1,8-diamine), which by contrast with its air-unstable oily neutral precursor, *nido*-6-NB<sub>9</sub>H<sub>12</sub>, is a yellow air-stable solid. Here we report that the reaction of this salt with [RhCl(PPh<sub>3</sub>)<sub>3</sub>] affords orange [8,8-(PPh<sub>3</sub>)<sub>2</sub>-*nido*-8,7-RhNB<sub>9</sub>H<sub>11</sub>] (compound **1**). In related work, the reaction of [Me<sub>4</sub>N][*nido*-6-CB<sub>9</sub>H<sub>12</sub>] with [*cis*-PtCl<sub>2</sub>(PMe<sub>2</sub>Ph)<sub>2</sub>] in the presence of methanol yields yellow [9-(OMe)-8,8-(PMe<sub>2</sub>Ph)<sub>2</sub>-*nido*-8,7-PtCB<sub>9</sub>H<sub>10</sub>] **2**, the B(9)-methoxy derivative of previously reported [8,8-(PMe<sub>2</sub>Ph)<sub>2</sub>-*nido*-8,7-PtCB<sub>9</sub>H<sub>11</sub>] **3**.<sup>2</sup>

Metallaheteroboranes **1** and **2** are new examples of polyhedral boron-containing compounds that are similarly anomalous in terms of a simplistic approach to cluster electron counting, and may therefore shed additional light on the interpretive problems often associated with compounds such as **4** and **5** as mentioned above. The rhodaazaborane **1** is fluxional with a mechanism that mirrors the one proposed for the rhodathaborane **4** and the platinacarborane **3** mentioned above. In contrast, the methoxy-substituted platinacarborane **2** does not exhibit dynamic behavior up to 398 K, suggesting that the presence of the methoxy-substituent increases the activation energy of the process. As part of this work, DFT calculations on the models [8,8-(PH<sub>3</sub>)<sub>2</sub>-*nido*-8,7-RhNB<sub>9</sub>H<sub>11</sub>] (**1a**) and [8,8-(PH<sub>3</sub>)<sub>2</sub>-*nido*-8,7-RhSB<sub>9</sub>H<sub>10</sub>] (**4a**) provide further insights regarding the relative stabilities of the *nido* versus the *closo* geometrical configurations in these types of eleven-vertex systems, and also regarding the intermediates that play a role in the fluxional process. The calculations demonstrate that 'agostic' types of interactions between the *exo*-polyhedral ligands and the rhodium atom are not required to attain the observed *nido* geometrical structures.

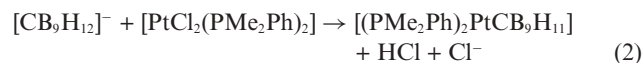
## Results and discussion

Reaction of [tmndH][*nido*-6-NB<sub>9</sub>H<sub>11</sub>] with [RhCl(PPh<sub>3</sub>)<sub>3</sub>] in dichloromethane solution at room temperature leads to the formation of orange [8,8-(PPh<sub>3</sub>)<sub>2</sub>-*nido*-8,7-RhNB<sub>9</sub>H<sub>11</sub>] **1** in 24% yield [eqn (1)].

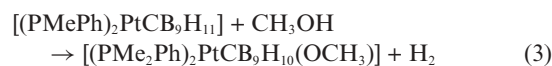


It has been previously reported that the reaction between the [*arachno*-6-CB<sub>9</sub>H<sub>14</sub>]<sup>-</sup> anion and *cis*-[PtCl<sub>2</sub>(PMe<sub>2</sub>Ph)<sub>2</sub>] in dichloromethane at room temperature affords yellow [8,8-(PMe<sub>2</sub>Ph)<sub>2</sub>-*nido*-8,7-PtCB<sub>9</sub>H<sub>11</sub>] (**3**, 46–64%) and pale yellow [9,9-(PMe<sub>2</sub>Ph)<sub>2</sub>-*arachno*-9,6-PtCB<sub>9</sub>H<sub>12</sub>] (0–3%), as major and minor

products respectively.<sup>2</sup> We now find that **3**, in lower yield, also results from use of the [*nido*-6-CB<sub>9</sub>H<sub>12</sub>]<sup>-</sup> anion rather than the corresponding *arachno* anion as reagent in the reaction with the platinum complex [eqn (2)].



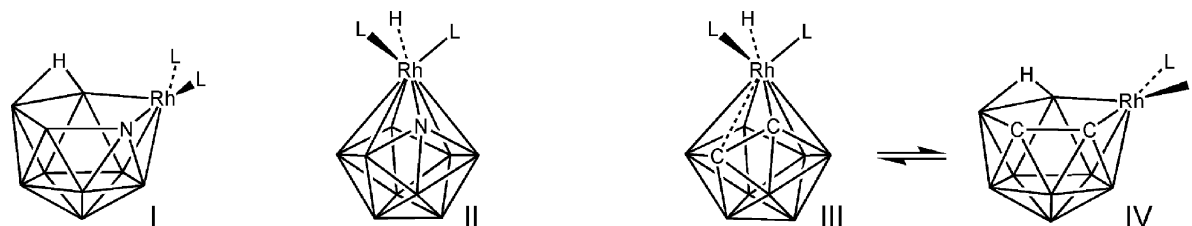
We have also found that the stirring of a solution of *nido*-8,7-platinamonocarborane **3** with methanol at room temperature results in the formation of the B-methoxy derivative [9-(OMe)-8,8-(PMe<sub>2</sub>Ph)<sub>2</sub>-*nido*-8,7-PtCB<sub>9</sub>H<sub>10</sub>] (**2**) in quantitative yield [eqn (3)].



The methoxy compound **2** can be directly prepared in a slightly more favorable overall yield (20% versus 12%) if the reaction between the [Me<sub>4</sub>N][CB<sub>9</sub>H<sub>12</sub>] salt and the platinum complex is carried out in dry methanol solvent.

In these syntheses [eqn (1) and (2)], the complete mechanism is unclear, but one possibility could be *via* an initial coordination of the *nido*-6-monoheteroborane anion to the sixteen-electron transition-element complex through hydridic B–H sites, generating intermediates with *exo*-polyhedral M–H–B bonds that can undergo cluster insertion and elimination of chlorine [eqn (1) and (2)]. Interestingly, the reaction of the [*nido*-6-NB<sub>9</sub>H<sub>11</sub>]<sup>-</sup> anion with the rhodium(t) complex, [RhCl(PPh<sub>3</sub>)<sub>3</sub>], to give *nido* species **1** does not appear to proceed with an oxidative addition of the bridging hydrogen atom to the rhodium centre. This would lead to the formation of the rhodium(III) isomer [1,1-(PPh<sub>3</sub>)<sub>2</sub>-1-H-*closo*-1,2-RhNB<sub>9</sub>H<sub>10</sub>] (schematic II) rather than the *nido* isomer (schematic I) as observed. This contrasts to isoelectronic [9,9-(PEt<sub>3</sub>)<sub>2</sub>-*nido*-9,7,8-RhC<sub>2</sub>B<sub>8</sub>H<sub>11</sub>] that exists as its *closo* isomer III in the solid state, although the *nido* form IV is observed to be in equilibrium with the *closo* species in solution over a wide range of temperatures.<sup>11</sup>

In this context, the dynamic behaviour of the rhodaazaborane compound **1** (see below near Scheme 1) may well proceed through a reversible internal redox reaction, involving the conversion of the B(9)–H–B(10) bridging hydrogen atom to RhH terminal in a *nido*–*closo*–*nido* sequence. In contrast to the rhodadicarborane system (III ⇌ IV), the *nido* configuration is the only one detected in the rhodaazaborane system. The energetic reasons for this difference in behaviour will be quite subtle, and involve the electronic properties of the heteroborane ligands (there will be a greater localization of charge on the one N heteroatom compared to two C heteroatoms) and the differential properties of PEt<sub>3</sub> versus PPh<sub>3</sub> ligands. In either case, it is clear that the *nido* versus *closo* energetic differences can be small in these systems. An interesting effect of this is that the observed *nido* configuration of compound **1** apparently conflicts with its formal *closo* electron count. This



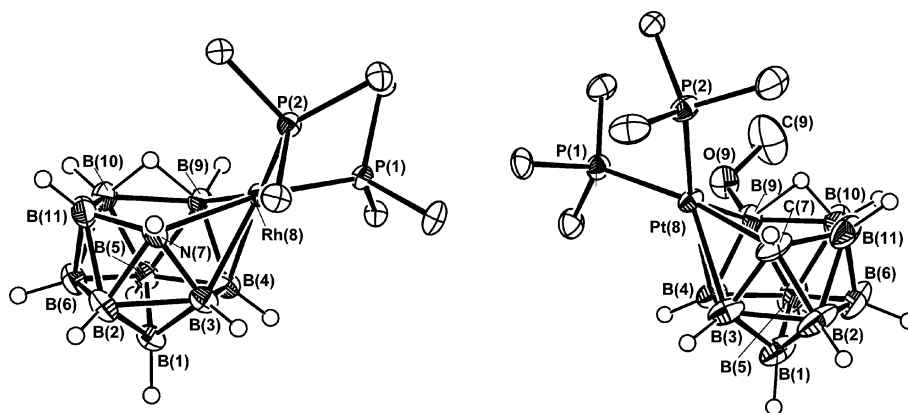


**Fig. 1** ORTEP-type of drawings of (left) [8,8-(PPh<sub>3</sub>)<sub>2</sub>-nido-8,7-RhNB<sub>9</sub>H<sub>11</sub>] **1** and (right) one member of the enantiomeric pair in the unit cell of [9-(OMe)-8,8-(PMe<sub>2</sub>Ph)<sub>2</sub>-closo-8,7-PtCB<sub>9</sub>H<sub>10</sub>] **2**.

**Table 1** Selected interatomic distances (Å) for **1** and **2** with estimated standard uncertainties (s.u) in parentheses. Corresponding calculated distances for the model compound [8,8-(PH<sub>3</sub>)<sub>2</sub>-nido-8,7-RhNB<sub>9</sub>H<sub>11</sub>] **1a** are given in square brackets.

(a) From the metal atom		Compound <b>2</b> : Molecule 1	
Compound <b>1</b>		P(1)–Pt(8)	2.271(3)
P(1)–Rh(8)	2.2332(8) [2.246]	P(2)–Pt(8)	2.351(3)
P(2)–Rh(8)	2.4163(8) [2.399]	B(3)–Pt(8)	2.305(7)
B(3)–Rh(8)	2.208(3) [2.296]	B(4)–Pt(8)	2.252(7)
B(4)–Rh(8)	2.230(3) [2.269]	B(9)–Pt(8)	2.312(6)
B(9)–Rh(8)	2.205(3) [2.259]	C(7)–Pt(8)	2.160(7)
N(7)–Rh(8)	2.231(2) [2.256]		
(b) Heteroatom–boron		Compound <b>2</b> : Molecule 1	
Compound <b>1</b>		C(7)–B(2)	1.673(9)
N(7)–B(2)	1.663(4) [1.673]	C(7)–B(3)	1.646(9)
N(7)–B(3)	1.596(4) [1.592]	C(7)–B(11)	1.590(9)
N(7)–B(11)	1.545(4) [1.548]		
(c) Boron–boron		Compound <b>2</b> : Molecule 1	
Compound <b>1</b>		B(2)–B(1)	1.758(10)
B(2)–B(1)	1.760(5) [1.751]	B(6)–B(1)	1.817(11)
B(6)–B(1)	1.812(5) [1.823]	B(5)–B(1)	1.764(10)
B(5)–B(1)	1.787(5) [1.786]	B(4)–B(3)	1.865(9)
B(4)–B(3)	1.841(5) [1.840]	B(11)–B(10) (longest)	1.960(10)
B(11)–B(10) (longest)	1.881(5) [1.910]	B(9)–B(4)	1.809(9)
B(9)–B(4)	1.765(5) [1.784]	B(10)–B(9)	1.811(10)
B(10)–B(9)	1.835(5) [1.807]	B(6)–B(2) (shortest)	1.737(11)
B(6)–B(2) (shortest)	1.734(5) [1.748]		
(d) Others		Compound <b>2</b> : Molecule 1	
Compound <b>2</b> : Molecule 1		C(9)–O(9)	1.430(6)
B(9)–O(9)	1.376(7)		

is due to a preference for rhodium to adopt a sixteen-electron configuration,<sup>7</sup> as discussed below.

The crystal and molecular structures of **1** and **2** were determined by X-ray diffraction analysis (Fig. 1). The molecular structures are consistent with the NMR data described below, thus confirming that the crystals selected were representative of the bulk samples. Selected interatomic distances are summarized in Table 1 and angles in Table 2. Crystallographic collection data are in Table 3.

Both metallaheteroboranes have the classical eleven-vertex *nido* cluster geometry which may be derived from an icosahedron by the removal of one vertex. The hetero and metal atoms are in adjacent positions on the open face. In each case, there is a hydrogen atom on the open-face bridging the B(9)B(10) site, as located by the X-ray diffraction analyses and confirmed by NMR spectroscopy. Selected dimensions of azarhodaundecaborane compound **1** may be compared to those of the isoelectronic and isostructural thiarhodaundecaborane [8,8-(PPh<sub>3</sub>)<sub>2</sub>-nido-8,7-RhSB<sub>9</sub>H<sub>10</sub>] **4**.<sup>1</sup> All

the cluster distances appear to be within the same ranges, apart from the shorter distances to the nitrogen atom in comparison with that of the sulfur atom, consistent with the smaller size of the former (covalent radii: 0.70 Å for N, 1.04 Å for S).

Compound **2** crystallises with two independent molecules in the unit cell, arranged as enantiomeric pairs, which differ chiefly in the torsion angles of the methoxy group on B(9) and of one of the phosphine ligands at the platinum centre. The presence of the methoxy substituent results in elongation of the Pt(8)–B(9) and Pt(8)–B(3) distances of 0.028 Å and 0.038 Å, respectively, and contraction of Pt(8)–C(7) by *ca.* 0.028 Å, with respect to the unsubstituted parent [8,8-(PMe<sub>2</sub>Ph)<sub>2</sub>-nido-8,7-PtCB<sub>9</sub>H<sub>11</sub>] **3**.<sup>2</sup> The other cage dimensions are similar, with B(10)–B(11) being the longest interboron distance in both platinamonocarborane clusters. The value of 1.376(7) Å for the O(9)–B(9) bond is within the reported range of 1.331 to 1.407 Å for exopolyhedral methoxy–boron linkages.<sup>12</sup>

**Table 2** Selected angles ( $^{\circ}$ ) between interatomic vectors for **1** and **2** with standard uncertainties (s.u). Corresponding calculated angles for the model compound [8,8-(PH<sub>3</sub>)<sub>2</sub>-*nido*-8,7-RhNB<sub>9</sub>H<sub>11</sub>] **1a** are given in square brackets.

(a) About the metal atom			
Compound <b>1</b>			Compound <b>2</b> : Molecule 1
P(1)–Rh(8)–P(2)	97.65(3) [95.27]	P(1)–Pt(8)–P(2)	96.1(1)
B(3)–Rh(8)–P(1)	128.54(9) [126.49]	B(3)–Pt(8)–P(1)	129.5(2)
B(3)–Rh(8)–P(2)	111.60(9) [125.64]	B(3)–Pt(8)–P(2)	120.6(2)
B(4)–Rh(8)–P(1)	93.30(9) [89.91]	B(4)–Pt(8)–P(1)	95.5(2)
B(4)–Rh(8)–P(2)	159.80(9) [173.16]	B(4)–Pt(8)–P(2)	168.0(1)
B(3)–Rh(8)–B(4)	49.00(12) [47.54]	B(3)–Pt(8)–B(4)	48.3(2)
N(7)–Rh(8)–P(1)	170.60(7) [166.37]	C(7)–Pt(8)–P(1)	171.7(1)
N(7)–Rh(8)–P(2)	88.81(7) [97.78]	C(7)–Pt(8)–P(2)	87.3(2)
N(7)–Rh(8)–B(3)	42.15(11) [40.93]	C(7)–Pt(8)–B(3)	43.1(2)
N(7)–Rh(8)–B(4)	78.57(11) [76.78]	C(7)–Pt(8)–B(4)	80.9(3)
N(7)–Rh(8)–B(9)	86.29(11) [86.34]	C(7)–Pt(8)–B(9)	92.8(3)
B(9)–Rh(8)–P(1)	91.57(9) [86.55]	B(9)–Pt(8)–P(1)	90.0(2)
B(9)–Rh(8)–P(2)	148.91(9) [138.24]	B(9)–Pt(8)–P(2)	136.4(1)
B(9)–Rh(8)–B(3)	84.48(12) [83.33]	B(9)–Pt(8)–B(3)	85.8(3)
B(9)–Rh(8)–B(4)	46.76(12) [46.41]	B(9)–Pt(8)–B(4)	46.7(2)
(b) About the cage heteroatom atom			
Compound <b>1</b>		Compound <b>2</b> : Molecule 1	
B(2)–N(7)–Rh(8)	129.2(2)	B(2)–C(7)–Pt(8)	126.4(4)
B(3)–N(7)–Rh(8)	68.18(14)	B(3)–C(7)–Pt(8)	73.1(4)
B(3)–N(7)–B(2)	68.2(2)	B(3)–C(7)–B(2)	64.1(4)
B(11)–N(7)–Rh(8)	116.1(2)	B(11)–C(7)–Pt(8)	108.1(4)
B(11)–N(7)–B(2)	67.6(2)	B(11)–C(7)–B(2)	67.3(4)
B(11)–N(7)–B(3)	120.3(2)	B(11)–C(7)–B(3)	116.1(5)
(c) About the OMe in compound <b>2</b> molecule 1			
O(9)–B(9)–B(4)	128.0(5)	O(9)–B(9) Pt(8)	113.0(4)
O(9)–B(9)–B(10)	123.7(5)	O(9)–B(9) B(5)	129.4(5)
C(9)–O(9)–B(9)	119.5(5)		

**Table 3** Crystallographic data for [8,8-(PPH<sub>3</sub>)<sub>2</sub>-*nido*-8,7-RhNB<sub>9</sub>H<sub>11</sub>] (compound **1**) and [9-(OMe)–8,8-(PMe<sub>2</sub>Ph)<sub>2</sub>-*nido*-8,7-PtCB<sub>9</sub>H<sub>10</sub>] (compound **2**)

Compound	<b>1</b>	<b>2</b>
Formula	C <sub>36</sub> H <sub>41</sub> B <sub>9</sub> ClNP <sub>2</sub> Rh.1/2CH <sub>2</sub> Cl <sub>2</sub>	C <sub>18</sub> H <sub>35</sub> B <sub>9</sub> OP <sub>2</sub> Pt
<i>M</i>	792.30	621.80
Crystal system	Triclinic	Monoclinic
<i>a</i> /Å	9.7567(12)	18.217(2)
<i>b</i> /Å	11.936(2)	13.785(2)
<i>c</i> /Å	17.698(2)	20.778(4)
<i>a</i> /°	93.138(9)	—
<i>β</i> /°	94.637(9)	99.89(1)
<i>γ</i> /°	105.790(9)	—
<i>D<sub>c</sub></i> /g cm <sup>-3</sup>	1.335	1.61
<i>U</i> /Å <sup>3</sup>	1970.4(5)	5140.3(14)
Space group	<i>P</i> $\bar{1}$	<i>P</i> 2 <sub>1</sub> / <i>a</i>
<i>Z</i>	2	8
<i>F</i> (000)	808	2431.87
Colour, habit	Yellow blocks	Yellow blocks
Crystal dimensions/mm	0.6 × 0.4 × 0.15	0.465 × 0.25 × 0.20
<i>μ</i> /mm <sup>-1</sup>	0.610	5.648
2 $\theta$ limits/°	3.0–50.0	4.0–50.0
No. of reflections: Total	8429	9459
Unique ( <i>R</i> <sub>int</sub> )	6954 (0.0397)	—
Observed [ <i>I</i> > 2 $\sigma$ ( <i>I</i> )]	5884	7161
Min., max. transmissions	0.7109, 0.914	0.1493, 0.4873
No. parameters	502	623
<i>R</i> (observed data)	0.0347	0.0211
<i>wR</i> (observed data)	0.0861	0.0269

Common parameters: Stoe STADI4 diffractometer, collected at 200(2) K. Mo-K $\alpha$  radiation (0.71073 Å), scan mode  $\omega$ - $\theta$ , scan width 1.05 + *a*-doublet splitting. Absorption correction azimuthal  $\Psi$  scans.

There is a substantial tilt of the M(8) vertex out of the plane of the open faces in **1** and **2**, with the angles between {M(8)E(7)B(9)} (where M = Rh, E = N; M = Pt, E = C) and {B(2)B(5)E(7)B(9)} (where E = N or C) being 37.98(17) $^{\circ}$  and 36.36(14) $^{\circ}$  respectively.

These values are close to the 36.6(2) $^{\circ}$  angle reported for [8,8-(PMe<sub>2</sub>Ph)<sub>2</sub>-*nido*-8,7-PtCB<sub>9</sub>H<sub>11</sub>] (**3**). The {M(PR<sub>3</sub>)<sub>2</sub>} moiety (where M = Rh, R<sub>3</sub> = Ph<sub>3</sub>; M = Pt, R<sub>3</sub> = Me<sub>2</sub>Ph) is twisted away from a reference plane through M(8)B(1)B(6), with the

dihedral angles between  $\{M(8)P(1)P(2)\}$  (where  $M = \text{Rh}$  or  $\text{Pt}$ ) and  $\{E(7)M(8)B(9)\}$  (where  $E = \text{C}$  or  $\text{N}$ ) being  $31.3(1)^\circ$  for **1** and  $43.8(1)^\circ$  for **2**. It is noteworthy that the phosphine ligands, which are almost exactly *trans* to the heteroatom groups (*i.e.* *trans* to HC, HN) have substantially shorter phosphorus–metal distances than the phosphine groups *trans* to the boron sides of the  $E(7)B(3)B(4)B(9)$  faces (where  $E = \text{CH}, \text{NH}$ ): 2.2332(8) versus 2.4163(8) Å for **1**, and 2.275(3) versus 2.353(3) Å for **2**. This structural feature is reflected in a large difference between the coupling constants  $^1J(M-^{31}\text{P})$  (where  $M$  is  $^{103}\text{Rh}$  or  $^{195}\text{Pt}$ ) within each of **1** and **2**, with the bigger value in each case corresponding to the shorter metal-to-phosphorus distance  $M(8)-P(1)$ .

The measured NMR data for  $[8,8-(\text{PPh}_3)_2\text{-nido-8,7-RhNB}_9\text{H}_{11}]$  **1** (Table 4, A) are consistent with the observed structure, although the broadness of the peaks at the lower temperature of 253 K precluded a complete resolution of the  $^{11}\text{B}$  spectrum at available field strengths. At this low temperature the  $^{11}\text{B}$  NMR spectrum shows six broad peaks that correspond to nine independent resonance positions, of which three are accidentally coincident in the observed peak at *ca.* +10.7 ppm and two accidentally coincident in the observed peak at *ca.* –19.2 ppm, giving the apparent 3 : 1 : 1 : 1 : 2 : 1 intensity-ratio pattern.

The assignments given in Table 4 for the resonances are reasonably based on their relative intensities, and by comparison with the previously reported rhodathiaborane,  $[8,8-(\text{PPh}_3)_2\text{-nido-8,7-RhSB}_9\text{H}_{10}]$ .<sup>1</sup> The assignments were supported by DFT calculations on model compound  $[8,8-(\text{PH}_3)_2\text{-nido-8,7-RhNB}_9\text{H}_{11}]$  **1a** (see below). These considerations, together with a detailed examination of the variable temperature multielement NMR properties of **1**, also allowed an identification of the pairs of exchanging boron sites which arise from the known fluxional behaviour of these eleven-vertex systems at elevated temperatures.<sup>1</sup> Thus, measurement at the higher temperature of 370 K reveals a substantial change in the  $^{11}\text{B}$  spectrum, which now exhibits six resonances in a 1 : 2 : 2 : 1 : 2 : 1 relative intensity ratio (Table 4, B). Additional evidence of the fluxional nature of this compound is gained from the  $^{31}\text{P}$  spectrum: the lower-temperature spectrum (203 K) consists of two doublets of doublets, with  $^1J(^{103}\text{Rh}-^{31}\text{P})$  for

one resonance being larger than the corresponding coupling for the other  $^{31}\text{P}$  nucleus and thereby enabling the assignment of P(1) as *trans* to the more electronegative nitrogen atom.<sup>13</sup> As mentioned above, this increase in magnitude of the couplings is associated with a contracted rhodium–phosphorus distance. The  $^{31}\text{P}(2)$  resonance is slightly broader, indicating a larger coupling  $^2J(^{31}\text{P}-\text{Rh}-^{11}\text{B})$  to  $^{11}\text{B}(4)$  and  $^{11}\text{B}(9)$  versus any  $^2J(^{31}\text{P}-\text{Rh}-^{14}\text{N})$  coupling to  $^{14}\text{N}(7)$ . At higher temperature fluxional site exchange for the two  $^{31}\text{P}$  doublets is apparent, as indicated by their coalescence into one doublet at 270 K in the 40.3 MHz spectrum. As just mentioned, the assignment of the  $^{11}\text{B}$  NMR data is supported by the GIAO-calculated nuclear magnetic chemical shielding properties on the model compound  $[8,8-(\text{PH}_3)_2\text{-nido-8,7-RhNB}_9\text{H}_{11}]$  **1a** (Table 6).

In contrast to compound **1**, the  $^{11}\text{B}$  NMR spectrum of  $[9-(\text{OMe})-8,8-(\text{PMe}_2\text{Ph})_2\text{-nido-8,7-PtCB}_9\text{H}_{10}]$  (**2**) at room temperature is sharper (Table 5). This difference arises because the  $\text{PMe}_2\text{Ph}$  ligand is less bulky than  $\text{PPh}_3$ : the molecule therefore tumbles more rapidly in solution and the  $^{11}\text{B}$  relaxation times are correspondingly longer. In this case, the assignments are readily made based on  $^1\text{H}-\{^{11}\text{B}(\text{selective})\}$  experiments, and by comparison with the unsubstituted congener,  $[8,8-(\text{PMe}_2\text{Ph})_2\text{-nido-8,7-PtCB}_9\text{H}_{10}]$  (**3**). Boron-site exchange was not observed up to 398 K, indicating a higher activation energy for the fluxional process in this methoxy substituted species **2** compared to its unsubstituted equivalent **3**, in which fluxionality is observed above 313 K. The  $^{31}\text{P}$  spectrum of compound **2** is assigned in a similar manner to that for **1**, and, additionally,  $^1\text{H}-\{^{31}\text{P}(\text{selective})\}$  experiments enable assignments among the four non-equivalent  $\text{PMe}$  groups on the two prochiral  $\text{PMe}_2\text{Ph}$  phosphine ligands. Incidental to this,  $^1\text{H}-\{^{31}\text{P}\}$  spectrum decoupling experiments on the  $^{195}\text{Pt}$  satellites in the  $^1\text{H}$  spectrum confirmed  $^3J(^{195}\text{Pt}-\text{P}-\text{C}-^1\text{H})$  to be positive, relative to  $^1J(^{195}\text{Pt}-^{31}\text{P})$  that can be taken to be positive.<sup>14</sup>

Potential information regarding the cluster bonding in these species may be gained from a comparative study of the shielding patterns of compound **1**, of the non-metallated neutral  $[\text{nido-6-NB}_9\text{H}_{12}]$ , of the  $[\text{arachno-6-NB}_9\text{H}_{13}]^-$  anion, and also of the previously reported iridaazaborane  $[9\text{-Cl-8-(}\eta^5\text{-C}_5\text{Me}_5\text{)-nido-8,7-IrNB}_9\text{H}_{11}]$  **6**.<sup>15</sup> This comparison is represented in Fig. 2. Thus, the

**Table 4**  $^{11}\text{B}$ ,  $^1\text{H}$  and  $^{31}\text{P}$  NMR data for  $[8,8-(\text{PPh}_3)_2\text{-nido-8,7-RhNB}_9\text{H}_{11}]$  (compound **1**)

(a) Cluster data				
A <sup>a</sup>		B <sup>b</sup>		
Assignment <sup>c</sup>	$\delta(^{11}\text{B})^d$ (ppm)	Assignment <sup>c</sup>	$\delta(^{11}\text{B})$ (ppm)	$\delta(^1\text{H})$ (ppm)
3, 9, 11 <sup>c</sup>	+10.7	9	+18.2	+4.79
6	–0.2	3,11	+9.3	+3.66
5	–13.1	1,6	–7.6	+2.83
4	–6.1	5	–9.9	+2.33
1,10 <sup>e</sup>	–19.2	4,10	–14.00	+1.96
2	–25.7	2	–25.5	+1.88
7	[NH]	7	[NH]	+2.58(br)
$\mu$ (9,10)				+0.09
(b) $^{31}\text{P}$ data <sup>f</sup>				
Assignment <sup>g</sup>	$\delta(^{31}\text{P})$ (ppm)	$^1J(^{103}\text{Rh}-^{31}\text{P})/\text{Hz}$	$^2J(^{31}\text{P}-^{31}\text{P})/\text{Hz}$	
P(1)	+50.7	+50.7	31.74	
P(2)	+19.5	+19.5		

<sup>a</sup>  $\text{CDCl}_3$  solution at 253 K. <sup>b</sup>  $\text{C}_6\text{D}_5\text{CD}_3$  solution at 370 K. <sup>c</sup> See text. <sup>d</sup>  $^1\text{H}-\{^{11}\text{B}(\text{selective})\}$  experiments were not carried out at low temperature. <sup>e</sup> Broadness of the peaks precludes the resolution of the individual resonances. <sup>f</sup>  $\text{CD}_2\text{Cl}_2$  solution at 203 K. <sup>g</sup> At higher temperature these two peaks collapse to one; coalescence temperature 270 K in the 40.3 MHz spectrum.

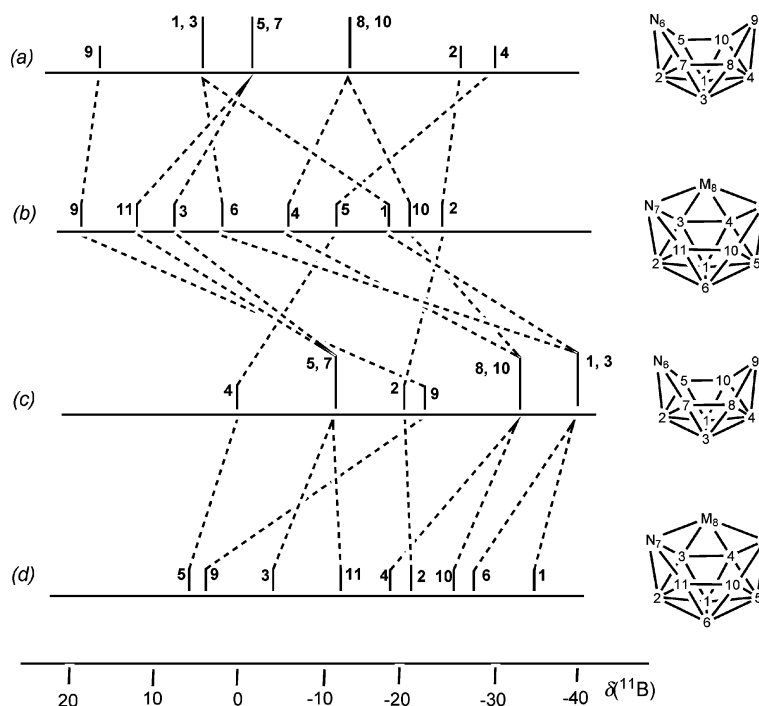
**Table 5**  $^{11}\text{B}$ ,  $^1\text{H}$  and  $^{31}\text{P}$  NMR data for compound [9-(OMe)-8,8-( $\text{PMe}_2\text{Ph}$ ) $_2$ -*nido*-8,7-PtCB $_9\text{H}_{10}$ ] **2** in  $\text{CDCl}_3$  at room temperature

(a) Cluster data					
Assignment <sup>a</sup>	$\delta(^{11}\text{B})$ (ppm)	$\delta(^1\text{H})$ (ppm)	$^1J(^{11}\text{B}-^1\text{H})/\text{Hz}$		
9	+28.3	OMe <sup>b</sup>			
11	+11.7	+3.28	<sup>c</sup>		
3	+10.0	+3.42	<sup>c</sup>		
6	-8.5	+2.06	133		
5	-11.4	+2.97	140		
4	-13.5	+1.74	192		
1	-15.1	+1.58 <sup>d</sup>	ca. 143 <sup>d</sup>		
2	-27.4	+1.52 <sup>f</sup>	ca. 173 <sup>d</sup>		
10	-29.2	+0.88	ca. 163 <sup>d</sup>		
7	[CH]	+3.60(br)			
$\mu$ (9,10)		+0.28			

(b) $\text{PMe}_2\text{Ph}$ data in $\text{CD}_2\text{Cl}_2$ solution at 237 K					
Assignment	$\delta(^{31}\text{P})$ (ppm)	$^1J(^{195}\text{Pt}-^{31}\text{P})/\text{Hz}$	$\delta(^1\text{H})$ (ppm)	$^3J(^{195}\text{Pt}-^1\text{H})/\text{Hz}$	$^2J(^{31}\text{P}-^1\text{H})/\text{Hz}$
P(1) (sh) <sup>g</sup>	-6.6	3287 Hz	A +1.92 B +1.55	32.0 Hz 26.4 Hz	11.7 Hz ca. 10.7 Hz
P(2) (br)	-4.5	2682 Hz	A +1.67 B +1.65	23.4 Hz 23.9 Hz	9.5 Hz ca. 9.5 Hz

<sup>a</sup> See text. <sup>b</sup> +3.71 ppm, <sup>d</sup> $J(^{195}\text{Pt}-^1\text{H}) = 2.6$  Hz. <sup>c</sup> Coupling constants not measured due to broadness of peaks relative to <sup>1</sup>J. <sup>d</sup> $^3J(^{195}\text{Pt}-^1\text{H}) = 24$  Hz. <sup>e</sup> Almost coincident peaks preclude more accurate values. <sup>f</sup> $^3J(^{195}\text{Pt}-^1\text{H}) = 37$  Hz. <sup>g</sup> $^2J(^{31}\text{P}_A-^{31}\text{P}_B) = 26.8$  Hz.

**Fig. 2** Stick diagrams of the chemical shifts and relative intensities in the  $^{11}\text{B}$  NMR spectra of (a) *nido*-6- $\text{NB}_9\text{H}_{12}$ , (b) [8,8-( $\text{PPh}_3$ ) $_2$ -*nido*-8,7-RhNB $_9\text{H}_{11}$ ] **1**, (c) [6-*arachno*-NB $_9\text{H}_{13}$ ] $^-$ , and (d) [9-Cl-8-( $\eta^5$ -C $_5$ Me $_5$ )-*nido*-8,7-IrNB $_9\text{H}_{11}$ ] **6**.

overall shielding of compound **1** [mean  $\delta(^{11}\text{B}) - 3.6$  ppm; diagram (b)] is much nearer to the *nido*-species [mean  $\delta(^{11}\text{B}) - 5.7$  ppm; diagram (a)] than to the *arachno* anion [mean  $\delta(^{11}\text{B}) - 15.4$  ppm; diagram (c)]. The shieldings at B(2)B(5) and B(1)B(6) in compound **1**, relative to the respective corresponding B(2,4) and B(1,3) positions in the non-metallated species, are of particular interest because a crossover of  $^{11}\text{B}$ (2,4) at lowest field and  $^{11}\text{B}$ (1,3) at highest field is characteristic of a ten-vertex *nido* to *arachno* change. In this regard, it can be seen in Fig. 2 that compound **1** [diagram (b)] retains the highest and lowest shieldings at B(2) and B(6), respectively [corre-

sponding to B(2) and B(3) in the non-metallated species], which is a general *nido* ten-vertex feature.<sup>16</sup> Conversely, in a comparison of [6-*arachno*-NB $_9\text{H}_{13}$ ] $^-$  with compound **6**, there is a crossover of  $^{11}\text{B}$ (1) at highest and  $^{11}\text{B}$ (5) at lowest shielding [corresponding to B(1) and B(4), respectively, in the non-metallated compounds] typical of an *arachno* ten-vertex cluster [diagram (c)]. Similar trends, as demonstrated elsewhere,<sup>2</sup> can be observed when [8,8-( $\text{PMe}_2\text{Ph}$ ) $_2$ -*nido*-8,7-PtCB $_9\text{H}_{11}$ ] is compared to the non-metallated *nido* and *arachno* [6-CB $_9\text{H}_{12}$ ] $^-$  and [6-CB $_9\text{H}_{14}$ ] $^-$  anions; these results can be extrapolated to the methoxy derivative dealt with in this paper.

This comparative NMR work suggests that the  $\{EB_9H_{10}X\}$  moiety (where E = C or N, X = H or OMe) in compounds **1** and **2**, although exhibiting some intermediate character on the heteroatom side to which the metal is bound, has more similarities to the non-metallated *nido* substrates  $[nido-6-EB_9H_{12}]^n$  (where E = C and  $n = -1$ ; or E = N and  $n = 0$ ), than to the non-metallated *arachno* ten-vertex substrates. These metallaheteroboranes may therefore be regarded as complexes of sixteen-electron  $\{Pt(PMe_2Ph)_2\}^{2+}$  and  $\{Rh(PPh_3)_2\}^+$  metal moieties with the corresponding  $\{nido-CB_9H_{10}(OMe)\}^{2-}$  and  $[nido-NB_9H_{11}]^-$  groups acting as *tetrahapto* ligands with bidentate character: this implies a two-orbital metal-to-heteroborane bonding interaction, and a corresponding basic four-orbital square-planar metal coordination sphere. This view of the eleven-vertex *nido*-clusters **1**–**4** as square-planar sixteen-electron complexes would imply that the metal site has Lewis acidic character in these compounds, consistent with the observed reactivity of these species with Lewis bases.<sup>4</sup>

By contrast, the  $^{11}B$  shielding pattern previously reported for the azaborane fragment of the eleven-vertex species  $[9-Cl-8-(\eta^5-C_5Me_5)-nido-8,7-IrNB_9H_{11}]$  **6**,<sup>15</sup> also shown in Fig. 2, diagram (d), better resembles the pattern of the  $[arachno-6-NB_9H_{13}]^-$  anion, with the retention at highest and lowest field of the B(6)B(1) and B(2)B(5) resonances, respectively [corresponding to B(1,3) and B(2,4) in the non-metallated *arachno* species; diagram (c)], a characteristic feature of ten-vertex *arachno*-compounds. This resemblance suggests that the iridium-to-azaborane bonding in this species could be described in terms of an iridium complex between  $\{Ir(\eta^5-C_5Me_5)\}^{2+}$  and tridentate *tetrahapto*  $\{arachno-NB_9H_{11}Cl\}^{2-}$ , with a three-orbital contribution to the cluster framework from the formally octahedral iridium(III).

From the Wade–Williams electron-counting rules and cluster-geometry approach,<sup>3</sup> compounds **1** and **2** are 24-electron cluster

systems for which a *closo*-geometry is at first sight predicted by a basic application of these rules. However, both **1** and **2** have sixteen-electron metal centres, and a commonly adopted simplistic application of the polyhedral skeletal electron pair theory does not accommodate square-planar 16-electron metal groups, because, as generally interpreted, this treatment always assumes that the metal contributes three orbitals to the cluster bonding, which implies an eighteen-electron octahedral metal centre. By contrast, the iridaazaborane, **6**,<sup>15</sup> in which the iridium atom has in fact an eighteen-electron metal configuration and conforms with the three-orbital bonding assumption, agrees with the electron-counting formalism.

Fig. 3 compares the  $^{11}B$  shielding patterns for  $[8,8-(PPh_3)_2-nido-8,7-RhNB_9H_{11}]$  **1** and  $[8,8-(PMe_2Ph)_2-nido-8,7-PtCB_9H_{11}]$  **3** at high and low temperatures, and  $[9-(OMe)-8,8-(PMe_2Ph)_2-nido-8,7-PtCB_9H_{10}]$  **2** at room temperature. It is apparent that there is a general parallel in the  $^{11}B$  shielding properties of equivalent sites in the three species. The most significant deviation from this parallel arises from the methoxy substitution at the B(9) site [Fig. 3(c)], which results in a deshielding of ca. 15 ppm at that position ( $\alpha$  to OMe) and a concomitant shielding of ca. 10 ppm at B(6) ( $\gamma$  to the OMe), B(4) ( $\beta$  to the OMe) and B(10) ( $\beta$  to OMe). The shift of the B(9) resonance to higher frequencies is expected from the known substituent effect of an OMe group, which could arise from the inductive electron-withdrawing effect ( $-I$ , electron acceptance). Conversely, a degree of electron donation by the methoxy substituent could be reflected by the accompanying shift to lower frequencies of the  $\gamma$  and  $\beta$  positions, as proposed by Heřmánek.<sup>17</sup>

An interesting feature of eleven-vertex *nido*-metallaheteroboranes that incorporate sixteen-electron transition-element centres is their fluxional behaviour. Thus, in the species based on the *nido*- $[MEB_9H_{10}]$  unit [where M = Rh, E = NH (compound **1**) or

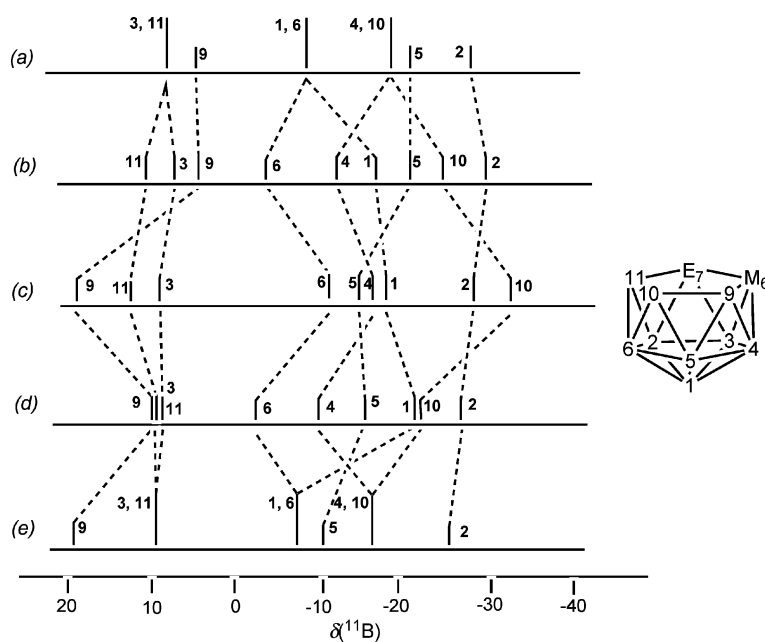


**Fig. 3** Stick representation of the  $^{11}B\{-^1H\}$  NMR spectra of compounds (a)  $[8,8-(PMe_2Ph)_2-nido-8,7-RhCB_9H_{11}]$  **3** at 383 K, (b)  $[8,8-(PMe_2Ph)_2-nido-8,7-RhCB_9H_{11}]$  **3** at room temperature, (c)  $[9-(OMe)-8,8-(PMe_2Ph)_2-nido-8,7-RhCB_9H_{10}]$  **2** at room temperature, (d)  $[8,8-(PPh_3)_2-nido-8,7-RhNB_9H_{11}]$  **1** at 253 K, and (e)  $[8,8-(PPh_3)_2-nido-8,7-RhNB_9H_{11}]$  **1** at 370 K.

S (compound **4**); and M = Pt, E = CH (compound **3**)], the six resonances corresponding to B(1) and B(6), B(3) and B(11) and B(4) and B(10) coalesce in pairs at higher temperatures, whereas B(2), B(5) and B(9) are unchanged. Coalescence temperatures yield  $\Delta G^\ddagger$  values of 48.4 kJ mol<sup>-1</sup> at 270 K for compound **1** and >75.0 kJ mol<sup>-1</sup> at  $T > 398$  K for compound **2**. In addition, <sup>31</sup>P-{<sup>1</sup>H} experiments at various temperatures on compound **1** demonstrate a concomitant exchange of the two triphenylphosphine ligands. These results resemble those for previously reported [8,8-(PMe<sub>2</sub>Ph)<sub>2</sub>-*nido*-8,7-PtCB<sub>9</sub>H<sub>10</sub>] **3** and [8,8-(PPh<sub>3</sub>)<sub>2</sub>-*nido*-8,7-RhSB<sub>9</sub>H<sub>10</sub>] **4**, which have activation energies  $\Delta G^\ddagger$  for the fluxional process of 62.6 kJ mol<sup>-1</sup> at 313 K (PMe <sup>1</sup>H resonance coalescence) and 58 kJ mol<sup>-1</sup> at 338 K (<sup>31</sup>P resonance coalescence), respectively.<sup>12</sup>

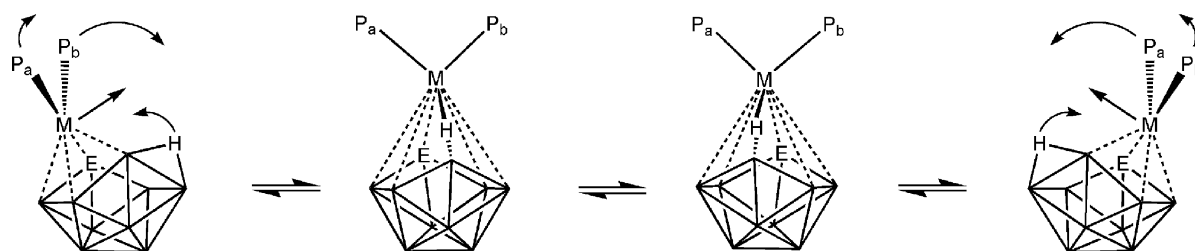
The coalescence of the <sup>11</sup>B resonances can be attributed to the {M(PR<sub>3</sub>)<sub>2</sub>} group (where M = Pt, R<sub>3</sub> = Me<sub>2</sub>Ph; Rh, R<sub>3</sub> = Ph<sub>3</sub>) moving across the formal {EB<sub>9</sub>H<sub>10</sub>} 'mirror plane', with a simultaneous reverse shift of the bridging hydrogen atom (Scheme 1). Concomitant exchange of the phosphine ligands in these species implies additional rotation of the {M(PR<sub>3</sub>)<sub>2</sub>} group (where R<sub>3</sub> = Ph<sub>3</sub> or PMe<sub>2</sub>Ph). For the compound [8,8-(PMe<sub>2</sub>Ph)<sub>2</sub>-*nido*-8,7-PtCB<sub>9</sub>H<sub>10</sub>] **3** it has been demonstrated that the four P-methyl proton resonances, a pair from each PMe<sub>2</sub>Ph ligand, coalesce in pairs giving two signals in the <sup>1</sup>H NMR spectrum.<sup>2</sup> This differs from a general rotation of the {Pt(PMe<sub>2</sub>Ph)<sub>2</sub>} unit above the {C(7)B(3)B(4)B(9)B(10)B(11)} face of the monocarbaborane fragment, which would lead to a single methyl proton resonance. Thus the complete dynamic process may be described as a shift of the platinum atom across the open face of the {CB<sub>9</sub>H<sub>10</sub>} cluster, linked with a half rotation of the {(PMe<sub>2</sub>Ph)<sub>2</sub>} ligand sphere (Scheme 1). Whereas the prochiral nature of the PMe<sub>2</sub>Ph phosphine in species of this type allows the identification of this half-rotation, the PPh<sub>3</sub> ligands in the rhodaheteroboranes [8,8-(PPh<sub>3</sub>)<sub>2</sub>-*nido*-8,7-RhEB<sub>9</sub>H<sub>10</sub>] (where E = NH or S) preclude such a complete assessment of the character of the phosphine interchange. Nevertheless, it is reasonable to assume that the half-rotational process occurs in a similar fashion in all these eleven-vertex [8,8-(L)<sub>2</sub>-*nido*-8,7-MEB<sub>9</sub>H<sub>10</sub>] species (where M = Rh, E = NH or S, L = PPh<sub>3</sub>; M = Pt, E = CH, L = PMe<sub>2</sub>Ph). In contrast, the methoxy-substituted platinacarbaborane, **2**, does not exhibit dynamic behaviour in either the <sup>11</sup>B or <sup>31</sup>P NMR spectra up to the maximum studied temperature of 398 K. The presence of the OMe substituent on the site adjacent to the metal centre obviously therefore inhibits a ready fluxionality.

## Calculations

Calculations using density functional theory methods (DFT) were carried out on the model rhodathiaboranes, [8,8-(PH<sub>3</sub>)<sub>2</sub>-*nido*-8,7-RhEB<sub>9</sub>H<sub>10</sub>] [where E = NH (**1a**), or S (**4a**)]. Calculated properties include (i) the geometries of the clusters, (ii) approximate relative energies of ground states and intermediates, and (iii) nuclear magnetic chemical shielding properties using the GIAO approach. The gross initial atomic coordinates for **1a** and **4a** were taken, with appropriate modifications, from unrelated eleven-vertex metallaheteroborane models such as [(PH<sub>3</sub>)<sub>2</sub>PtB<sub>10</sub>H<sub>12</sub>], previously calculated in our laboratories. Selected energy-optimized interatomic separations and angles for the model [8,8-(PH<sub>3</sub>)<sub>2</sub>-*nido*-8,7-RhNB<sub>9</sub>H<sub>10</sub>] **1a** are given in parentheses in Tables 3 and 4 respectively, together with the experimentally determined data for [8,8-(PPh<sub>3</sub>)<sub>2</sub>-*nido*-8,7-RhNB<sub>9</sub>H<sub>10</sub>] **1**. Data for [8,8-(PH<sub>3</sub>)<sub>2</sub>-*nido*-8,7-RhSB<sub>9</sub>H<sub>10</sub>] **4a** are listed in the ESI.†

The agreement between the computed interatomic distances for **1a** and those for the crystallographically characterized compound **1** is satisfactory. The calculated Rh–B(3) separation in **1** is 0.09 Å longer than the experimental one, whereas the Rh–B(4) and Rh–B(9) distances are only 0.04 Å and 0.05 Å longer, but these are not unreasonable for DFT-calculated interatomic distances involving second-row transition elements and currently available basis sets. A better agreement is found between the computed and experimental N–B and B–B distances as would be expected for first-row main-group elements. A reasonable measure of the validity of the calculated structures of these rhodaheteroboranes is given by a comparison of the measured <sup>11</sup>B NMR chemical shift values and the boron nuclear shielding properties as calculated *via* the GIAO approach. Thus, the <sup>11</sup>B chemical shifts calculated for **4a** reproduce the experimental trend, and are sufficiently in agreement to confirm the previously reported assignments.<sup>1</sup> The most significant differences occur for the low-field resonances of the boron atoms B(3), B(9) and B(11) that are adjacent to the metal and hetero atoms.

The <sup>11</sup>B NMR spectrum of **1** was recorded for solutions in different solvents at 253 K and 370 K. As mentioned above, the low temperature spectrum is rather broad and precludes resolution of the nine individual resonances that are expected for the eleven-vertex asymmetric structure of the rhodaaazaborane. In the first instance it is therefore more instructive to compare the calculated values with the higher temperature spectrum that features narrower resonances, but for which the fluxional process



E = CH or NH; M = Rh or Pt

Scheme 1

**Table 6** Measured  $^{11}\text{B}$  chemical shifts ( $\delta$ , ppm) for [8,8-( $\text{PPh}_3$ ) $_2$ -*nido*-8,7-RhNB $_9$ H $_{11}$ ] **1** in  $\text{C}_6\text{D}_5\text{CD}_3$  solution at 370 K and [8,8-( $\text{PH}_3$ ) $_2$ -*nido*-8,7-RhSB $_9$ H $_{10}$ ] **4** in  $\text{CD}_2\text{Cl}_2$  at 298 K, compared with the corresponding calculated chemical shifts for their related P-hydril models **1a** and **4a**

Assignment	<b>1</b>		Assignment	<b>4a</b>	
	Exptl.	Calcd. (mean)		Exptl.	Calcd.
9	+18.2	+18.1	3	+16.3	+23.2
3,11	+9.3	+7.9, +11.4 (+9.7)	9	+12.6	+18.8
1,6	-7.6	-13.4, +2.5 (-5.5)	11	+6.0	+10.0
5	-9.9	-12.5	6	+4.5	+7.3
4,10	-14.0	-0.1, -21.0 (-10.6)	4	+2.5	+2.1
2	-25.5	-28.2	5	-9.3	-9.2
			1	-18.6	-17.5
			10	-21.1	-19.3
			2	-27.5	-28.7

averages the shifts of particular pairs of resonances as detailed above. The chemical shifts listed in Table 6 reveal a good correlation between the experimental and calculated values. This is particularly evident in the resonances due to the exchanging pairs of atoms B(3,11), B(1,6) and B(4,10) for which the calculated average values are close to the measured higher-temperature  $^{11}\text{B}$  chemical shifts for **1**.

The satisfactory agreement of the calculated and experimental structural and nuclear shielding properties for **1/1a** and **4/4a** suggests that DFT methods should provide a useful indication of the likely transition states in the dynamic behaviour referred to above. Therefore, the possible non-rigid intermediates through the proposed half-rotational metal-flip (Scheme 1) have been investigated using the calculated rhodathiaboranes [8,8-( $\text{PH}_3$ ) $_2$ -*nido*-8,7-RhEB $_9$ H $_{10}$ ] [where E is NH (**1a**) or S (**4a**)] as limiting structures in the fluxional pathway. We thence produced an initial model for **4a** using a transition state corresponding to one previously postulated for this type of system,<sup>1</sup> with a {RhH( $\text{PH}_3$ ) $_2$ } moiety capping the boat-shaped, six-membered face of the cluster (central diagrams of Scheme 1 above), with overall  $C_s$  symmetry. An initial energy minimization was carried out using the B3LYP methodology and the 6-31G\* basis sets. This minimization settled out into an 'isonido' type of cluster geometry (Fig. 4), which features a quadrilateral open face [S(7)Rh(8)B(9)B(10)], with the Rh(8)–B(10) distance being non-bonding at 2.83 Å (the initial *nido* numbering as in Fig. 1 is maintained). A frequency analysis showed no imaginary frequencies, suggesting that this structure represents a stable local minimum close to the starting postulated  $C_s$  transition-state model. Using this 'isonido' form in the STQN calculation thence produced a transition state (designated **TS**, Fig. 4) slightly higher in energy by *ca.* 1 kJ mol $^{-1}$ , with the {RhH( $\text{PH}_3$ ) $_2$ } moiety symmetrically positioned above the cluster, featuring a Rh(8)–H–B(9) bridging bond in a  $C_s$  *closo*-type eleven-vertex geometry (for simplicity the numbering for the *nido* clusters is maintained). The highest point of the computed reaction coordinate for the fluxionality therefore corresponds to the formation of a transient eleven-vertex *closo*-rhodathiaborane, **TS**, with a saddle point of order 1: the standard condition-free energy for **TS** is 49 kJ mol $^{-1}$  above the ground state (Fig. 4).

For the rhodaazaborane model [8,8-( $\text{PH}_3$ ) $_2$ -*nido*-8,7-RhNB $_9$ H $_{11}$ ] **1a**, by contrast, no saddle point was derivable in the STQN calculation, with the 'transition state' settling out as a local minimum with no imaginary frequencies: the energy differences between the 'closo' and 'isonido' conformations are too small to be significant at the level of calculation used. This

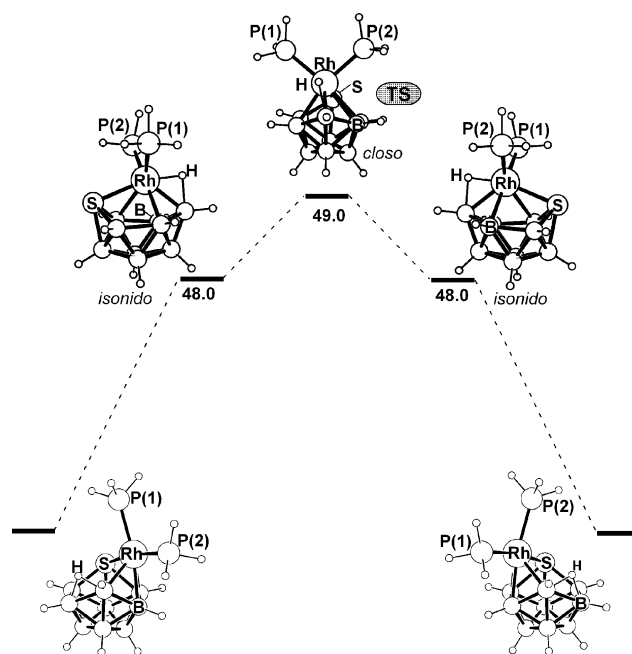


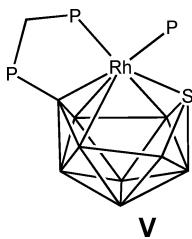
**Fig. 4** DFT-calculated energies (kJ mol $^{-1}$ ) and intermediates, computed at the B3LYP/6-31G\*/LANL2DZ level for the fluxional process of [8,8-( $\text{PH}_3$ ) $_2$ -*nido*-8,7-RhSB $_9$ H $_{10}$ ] **4a**.

finding now implies an activation energy of 23 kJ mol $^{-1}$  above the ground state, 26 kJ mol $^{-1}$  lower than the calculated value of 49 kJ mol $^{-1}$  for the sulfur compound **4a**. This qualitatively follows the experimentally measured trend:  $\Delta G^\ddagger$  for **4** being 58 kJ mol $^{-1}$ , *i.e.* 10 kJ mol $^{-1}$  higher than the 48 kJ mol $^{-1}$  determined experimentally for **1**. For **1a**, by contrast, the calculations did not find an *isonido*-structured intermediate close to the transition state, a further indication of the small differences of energy that can occur between the *isonido* and *closo* geometries in this eleven-vertex cluster area, as found for **4a**. An important factor behind the discrepancy between calculated and experimental  $\Delta G^\ddagger$  values is the different nature of the phosphine ligands in the model compounds and the synthesized compounds; on simplistic steric grounds, a higher activation energy may be expected for  $\text{PPh}_3$  versus  $\text{PH}_3$ .

The calculated intermediates in Fig. 4 represent points on a geometrical continuum of distortion from the eleven-vertex *nido* geometry to eleven-vertex *closo*-configuration as the metal centre undergoes a half-rotational flip from side to side above

the {S(6)B(3)B(4)B(9)B(11)B(10)} face, this face resembling a cyclohexane boat-type conformation. In this process, the B–H–B bridging hydrogen atom shifts to a Rh–H–B bridging position to attain a partial metal–hydride character in the transition state. To assess the alternative open-face rotation, for **4a** we calculated for a half-rotation of the {Rh(PH<sub>3</sub>)<sub>2</sub>} centre, in which the bridging hydrogen atom moves across through the sulfur side of the pentagonal open face (rather than motion *via* the boron side as illustrated in Scheme 1 and Fig. 4). The results of this calculation showed that this route may be disregarded, as the intermediate lies at considerably higher energy above the ground state, by *ca.* 92 kJ mol<sup>-1</sup>. This is not unexpected, because the lower-energy process (Fig. 4) allows the moving hydrogen atom to continue to be associated with the B(9) vertex in a B–H–M *pseudo*-bridging manner (H–B distance 1.54 Å; H–M distance 1.62 Å in TS) and thus retain the electron-pair in the Rh–H–B linkage in the cluster bonding. This has similarities to the situation observed in the crystallographic analyses and DFT calculations of the recently published series of ten-vertex *isonido*-iridadecaborane clusters, [(PPh<sub>3</sub>)<sub>2</sub>HIrB<sub>9</sub>H<sub>9</sub>(PPh<sub>3</sub>)].<sup>18</sup>

In terms of the calculated *isonido*-structured intermediates of Fig. 4, it may be noted that a directly analogous eleven-vertex *isonido* species, [1-PPh<sub>3</sub>-{1,3-(μ-dppm)}]-*isonido*-1,2-RhSB<sub>9</sub>H<sub>8</sub> (**7**), which features a quadrilateral {Rh(1)S(2)B(7)B(4)} open face, has previously been experimentally observed (schematic V).<sup>19</sup> The '*isonido*' type of distortion is also observed in formally *closo* {1,2,4-MC<sub>2</sub>B<sub>9</sub>} species as exemplified by [1,1,1-(PPh<sub>3</sub>)<sub>2</sub>H-1,2,4-IrC<sub>2</sub>B<sub>8</sub>H<sub>10</sub>] (*closo* eleven-vertex numbering system), and indicated by the hatched lines in schematic III above.<sup>20</sup> It is apparent that different ligands at the rhodium centre, often allied with variation of substituents on the boron cage, can stabilize *closo* geometries (*versus nido*) in the solid state, as for example in [3-(η<sup>1</sup>-dppm)-1,1-(η<sup>2</sup>-dppe)-*closo*-1,2-RhSB<sub>9</sub>H<sub>8</sub>].<sup>19</sup> These experimentally observed *isonido* and *closo* clusters can be notionally considered as "frozen snapshots" of the intermediates in the fluxional mechanism proposed here. There is also relevance to the reported cluster rearrangement that renders all the vertices equivalent on the NMR time scale in the *closo*-[B<sub>11</sub>H<sub>11</sub>]<sup>2-</sup> binary borane dianion.<sup>21</sup>



Overall, the observed *nido*-type geometries of **1**, **2**, **3** and **4**, with the B–H–B bridging hydrogen atom on the B(9)–B(10) edge, represent one of the limiting structures in an eleven-vertex *nido*–*isonido*–*closo* structural continuum that exhibits a rather smooth progression in the calculated structure/potential-energy surface. Thus, it is not surprising that changes in cluster substituents and constituents can lead to significant perturbations of the energy surface, favouring different configurations in the structural continuum. This is nicely exemplified by the parent rhodathiaborane **4**, in which a formal substitution of the BH(9) terminal hydrogen atom and the B(9)–H–B(10) bridging hydrogen

atom by a CO ligand (2 × H *versus* CO implies the same number of skeletal electrons) results in closure of the cluster to give the *closo*-structured compound, [1-(CO)-1,3-(PPh<sub>3</sub>)<sub>2</sub>-*closo*-1,2-RhSB<sub>9</sub>H<sub>8</sub>].<sup>4</sup> An analogous structural change is observed when the B(9)–B(10) bridging hydrogen atom of either [8,8-(PPh<sub>3</sub>)<sub>2</sub>-*nido*-8,7-RhSB<sub>9</sub>H<sub>10</sub>] **4** or [8,8-(dppe)-*closo*-8,7-RhSB<sub>9</sub>H<sub>10</sub>] **5** is removed as a proton by strong bases, affording the corresponding *closo* rhodathiaborane anions, [1,1-(PPh<sub>3</sub>)<sub>2</sub>-1,2-RhSB<sub>9</sub>H<sub>9</sub>]<sup>-</sup> and [1,1-(dppe)-*closo*-1,2-RhSB<sub>9</sub>H<sub>9</sub>]<sup>-</sup>,<sup>6</sup> with no change in cluster-electron count. On the other hand, incorporation of the bidentate phosphine dppm, which bridges the rhodium atom and the B(3)-boron vertex, favours the *isonido* configuration in **7** (schematic V above).<sup>19</sup>

A further example of the importance that ligands and heteroborane constituents have on the observed structure [and, by analogy, the bonding] in the eleven-vertex system is shown by the behaviour of the isoelectronic [9,9-(PET<sub>3</sub>)<sub>2</sub>-*nido*-9,7,8-RhC<sub>2</sub>B<sub>8</sub>H<sub>11</sub>] mentioned above. This compound exists as its *closo* isomer, [1,1-(PET<sub>3</sub>)<sub>2</sub>-1-(H)-1,2,3-RhC<sub>2</sub>B<sub>8</sub>H<sub>10</sub>] in the solid state, although the *nido* form is observed to be in an interesting equilibrium with the *closo* species in solution over a wide range of temperatures (schematics III, IV).<sup>11</sup>

It has been suggested,<sup>6</sup> and, interestingly, it seems to be currently accepted in recent primary organometallic reference works,<sup>5</sup> that an 'agostic' interaction of an electron-pair in the phosphine-bound *ortho*-hydrogen atoms (one electron from each PPh<sub>3</sub> ligand) with the rhodium atom in the rhodathiaborane **4** plays an important and decisive role in the stabilization of *nido* *versus closo* geometries in this type of compound. Moreover, it is proposed that, on deprotonation of **4** and **5**, the two Rh...H–C 'agostic' interactions somehow switch off, affording a *closo*-cluster geometry. However, it is not clear how two such interactions should be necessary to provide only two extra cluster electrons, since each of the two defined agostic interaction should involve a C–H *sigma* electron pair, thus involving a total of four electrons. As an alternative rationale, it has been pointed out that there is no need to invoke such 'agostic' interaction if the transition-element centre concerned is comfortable with a sixteen-electron configuration.<sup>7</sup> Germane to this question, the calculations presented here for **1a** and **4b**, with model PH<sub>3</sub> ligands, and which reasonably mirror the observed structures and NMR parameters of **1** and **4**, demonstrate that the clusters exhibit a *nido* structure in the ground state, *i.e.* as isolated molecules, without any possible contribution from *agostic* interactions from P-aryl hydrogen atoms or from other molecules. On the other hand, the experimental evidence indicates that the {MEB<sub>9</sub>} eleven-vertex system is rather flexible, the observed structures of the polyhedral clusters resulting from the balance of electronic changes promoted by either metal-bound ligands, boron substituents, or the presence of one or more bridging hydrogen atoms.

## Conclusions

Two new examples, [8,8-(PPh<sub>3</sub>)<sub>2</sub>-*nido*-8,7-RhNB<sub>9</sub>H<sub>11</sub>] **1** and [9-(OMe)-8,8-(PPh<sub>3</sub>)<sub>2</sub>-*nido*-8,7-PtCB<sub>9</sub>H<sub>10</sub>] **2** of *nido*-type eleven-vertex cluster geometry have been prepared and characterized. Their structures, NMR properties and fluxionalities have been compared with previously reported and closely related eleven-vertex 12-skeletal-electron-pair species, such as the platinacarborane **3** and the rhodathiaborane **4**. As part of this work,

it has been established that the tetramethylnaphthalene-1,8-diammonium salt of the [*nido*-6-NB<sub>9</sub>H<sub>11</sub>]<sup>−</sup> anion, *viz.* [tmndH]<sup>−</sup>[NB<sub>9</sub>H<sub>11</sub>], is an air-stable reagent that provides a convenient entry in the sparsely-examined area of metallazaboranes. Thus, compound **1** represents the first structurally characterized eleven-vertex *nido*-rhodaazaborane.

The previously proposed inter-enantiomeric fluxional behaviour in this eleven-vertex system, now nicely extended to include the nitrogen-containing cluster compound **1**, has been studied by DFT calculations. These studies reveal that *isonido*-shaped and *closo*-shaped clusters are points along the reaction coordinate in the fluxional process that interchanges the two ground-state enantiomeric eleven-vertex *nido*-cages. The potential-energy profiles of the system demonstrate that, for the compounds examined, the *nido* cluster configuration is more stable than either of the *isonido* or *closo* arrangements. The energy differences are small, however, and this rationalises some of the general observations within the eleven-vertex *nido*–*isonido*–*closo* structural continuum for sets of cluster compounds with ostensibly formally equivalent skeletal electron counts. The precise structures observed are largely governed by the variation of either the metal-bound ligands or the heteroborane cluster constituents or cluster substituents; as such, observed species do not necessarily adhere rigidly to the Wade–Williams cluster-geometry/electron-counting paradigm as it is often commonly interpreted. Prime factors are (a) the nature of the metal centre; preference for sixteen-electron *versus* eighteen-electron transition-element configurations can be a dominant factor here; and (b) the incidence or otherwise of hydrogen atoms that can act either as terminal metal hydrides or be localised in bridging positions on a cluster open face. In the systems studied, we found no evidence to support the proposed importance of Rh...C–H ‘agostic’ contacts or related interactions in dictating *nido* structures *versus* otherwise predicted *closo* geometries. In these cases, rather, the observed *nido* structures often reflect the preference of the relevant metal centres for sixteen-electron transition-element configurations rather than eighteen-electron configurations. For the fluxionalities, in the pathway between the limiting *nido*-shaped configurations, it seems likely that an internal switch between sixteen-electron and eighteen-electron transition-element centres may well play a significant role, involving a transient increase by +2 in the formal oxidation state of the metal centre (compare reference 22).

In twelve-vertex *closo*-metallaheteroborane compounds, a metal-to-heteroborane η<sup>5</sup>-rotation may be considered as a general fluxional process;<sup>23</sup> the fluxional mechanism delineated in this present work may similarly be regarded as a common behavioural process within the eleven-vertex *nido*-{MEB<sub>9</sub>}-cluster area when the metal is formally a square-planar sixteen-electron centre.

## Experimental

### General

The reagents *nido*-6-NB<sub>9</sub>H<sub>12</sub>,<sup>10</sup> [Me<sub>4</sub>N][*nido*-6-CB<sub>9</sub>H<sub>12</sub>],<sup>24</sup> [RhCl(PPh<sub>3</sub>)<sub>3</sub>]<sup>25</sup> and [*cis*-PtCl<sub>2</sub>(PMe<sub>2</sub>Ph)<sub>2</sub>],<sup>25</sup> were prepared by literature methods. *N,N,N',N'*-Tetramethylnaphthalene-1,8-diamine (tmnd) was obtained from commercial sources. The reactions were carried out under an inert atmosphere of dry nitrogen, although subsequent manipulations were carried out

in air. Dried and degassed solvents were used throughout. Preparative thin-layer chromatography (TLC) was carried out using 1 mm layers of silica gel G (Fluka, type GF254) made from water slurries on glass plates of dimensions 20 × 20 cm. Mass spectrometry was done on a V. G. AUTOSPEC instrument using fast-atom bombardment (FAB; Cs<sup>+</sup>-ion bombardment of a target solution in 3-nitrobenzyl alcohol; pressure gas phase 10<sup>−6</sup> mmHg).

### NMR spectroscopy

NMR spectroscopy was performed at 2.35 and/or 9.35 T on commercially available instrumentation, with the general techniques being essentially as detailed in other papers from our laboratories,<sup>26</sup> and using the general approach as most recently summarised in reference 27. Chemical shifts δ are given to high frequency (low field) of Ξ 100 MHz (SiMe<sub>4</sub>) for <sup>1</sup>H (quoted ±0.05 ppm), Ξ 40.480 730 MHz (nominally 85% H<sub>3</sub>PO<sub>4</sub>) for <sup>31</sup>P (quoted ±0.5 ppm) and Ξ 32.083 971 MHz (nominally F<sub>3</sub>BOEt<sub>2</sub> in CDCl<sub>3</sub>) for <sup>11</sup>B (quoted ±0.5 ppm), Ξ being defined as in reference 28. The chemical shifts were calibrated using solvent deuteron or residual proton resonances as internal secondary standards. Values for observed splittings arising from coupling constants <sup>1</sup>J(<sup>11</sup>B–<sup>1</sup>H) are given ± 4 Hz.

### Single-crystal X-ray diffraction analysis

Crystals of [8,8-(PPh<sub>3</sub>)<sub>2</sub>-8,7-*nido*-8,7-RhNB<sub>9</sub>H<sub>11</sub>] (compound **1**) and [9-(OMe)-8,8-(PMe<sub>2</sub>Ph)<sub>2</sub>-8,7-*nido*-8,7-PtCB<sub>9</sub>H<sub>10</sub>] (compound **2**) suitable for the X-ray analyses were grown from concentrated CH<sub>2</sub>Cl<sub>2</sub> solutions by liquid–liquid diffusion of hexane. For crystallographic details see Table 3.

CCDC reference numbers 637884 and 637885.

For crystallographic data in CIF or other electronic format see DOI: 10.1039/b702767b

### Computations

Calculations carried out in this study were performed using the Gaussian 98 and Gaussian 03 packages.<sup>29</sup> Structures were initially optimised with the STO-3G\* basis-sets for B, C, P, S, N, H and with the LANL2DZ basis-set for the metal atoms, using standard *ab initio* methods. The final optimisations, including frequency analyses to confirm the true minima, together with GIAO NMR nuclear-shielding predictions, were performed using B3LYP methodology, with the 6-31G\* and LANL2DZ basis-sets. GIAO NMR nuclear shielding predictions were performed on the final optimised geometries. In each case the compounds were modelled using hydrogen atoms rather than phenyl groups on the phosphine ligands in order to reduce computation time. In the results of all the structural calculations it is noted that all the distances from metal to boron are somewhat longer than those observed experimentally. We have found this to be a general feature in DFT calculations of the structure of metallaboranes of second- and third-row transition elements using the same basis-sets, for which we have reported on ruthenaboranes,<sup>30</sup> iridaboranes<sup>18</sup> and platinaboranes.<sup>30</sup> Other calculated intercluster connectivities, *e.g.* interboron distances, much more closely match those determined experimentally. Transition-state optimizations were carried out using the STQN method (synchronous transit-guided

quasi-Newton), which finds a transition state that connects two local minima on the potential energy surface.<sup>31</sup>

## Syntheses

**Synthesis of [tmndH][6-*nido*-NB<sub>9</sub>H<sub>11</sub>].** tmnd (1.7 g; 8 mmol) was added to a colourless solution of [*nido*-6-NB<sub>9</sub>H<sub>12</sub>] (1 g; 8 mmol) in hexane (*ca.* 50 ml). A pale yellow precipitate formed instantly. This product was separated by filtration and dried under vacuum. The yield of [tmndH][*nido*-6-NB<sub>9</sub>H<sub>11</sub>] was 2.0 g (74%). The salt is a yellow solid that, by contrast with its neutral precursor, is air stable.

**Synthesis of [8,8-(PPh<sub>3</sub>)<sub>2</sub>-8,7-*nido*-8,7-RhNB<sub>9</sub>H<sub>11</sub>] (compound 1).** [RhCl(PPh<sub>3</sub>)<sub>3</sub>] (200 mg; 0.22 mmol) was added to a solution of [tmndH][*nido*-6-NB<sub>9</sub>H<sub>11</sub>] (81 mg; 0.24 mmol) in dichloromethane at -79 °C [CO<sub>2</sub>(s)-acetone bath]. The reaction mixture was stirred with slow warming to room temperature (*ca.* 3 h). The resulting red solution was filtered through silica, reduced in volume (rotary evaporator), applied to preparative thin-layer chromatography TLC plates and developed using a 1 : 1 mixture of CH<sub>2</sub>Cl<sub>2</sub>-hexane as mobile phase. The chromatogram resulted in one orange band of *R<sub>f</sub>* = 0.13 that was extracted from the silica to give a component characterised as [8,8-(PPh<sub>3</sub>)<sub>2</sub>-8,7-*nido*-8,7-RhNB<sub>9</sub>H<sub>11</sub>] (compound 1; 39 mg; 0.05 mmol; 24%).

**Synthesis of [9-(OMe)-8,8-(PMe<sub>2</sub>Ph)<sub>2</sub>-8,7-*nido*-8,7-PtCB<sub>9</sub>H<sub>10</sub>] (compound 2).** [*cis*-PtCl<sub>2</sub>(PMe<sub>2</sub>Ph)<sub>2</sub>] (100 mg; 0.18 mmol) and [Me<sub>4</sub>N][*nido*-6-CB<sub>9</sub>H<sub>12</sub>] (39 mg; 0.2 mmol) were stirred in dry methanol (*ca.* 25 ml) for 5 h at room temperature, under an inert atmosphere of dry nitrogen. During this time the solution turned from colourless to yellow. The reaction mixture was filtered through silica, the silica washed through with CH<sub>2</sub>Cl<sub>2</sub>, and the combined liquid filtrates reduced to dryness. Preparative TLC using CH<sub>2</sub>Cl<sub>2</sub> (100%) as eluent gave two bands: (a) yellow (*R<sub>f</sub>* = 0.7), and (b) brown (*R<sub>f</sub>* = 0.5). Each band was removed from the plate and extracted with CH<sub>2</sub>Cl<sub>2</sub>. The former component was identified as [9-(OMe)-8,8-(PMe<sub>2</sub>Ph)<sub>2</sub>-*nido*-8,7-PtCB<sub>9</sub>H<sub>10</sub>] (compound 2; 8 mg; 0.045 mmol; 25%). The second component exhibited no <sup>11</sup>B NMR signals and was not further investigated. In an alternative reaction compound 2 (14 mg; 0.02 mmol) was obtained quantitatively by reaction of [8,8-(PMe<sub>2</sub>Ph)<sub>2</sub>-*nido*-8,7-PtCB<sub>9</sub>H<sub>11</sub>] (14 mg; 0.02 mmol) with methanol solvent (*ca.* 20 ml) at room temperature for 2 h. The non-methoxy substituted platinamonocarbaborane precursor was prepared in 12% yield by the reaction of [*cis*-PtCl<sub>2</sub>(PMe<sub>2</sub>Ph)<sub>2</sub>] (100 mg; 0.18 mmol) and [Me<sub>4</sub>N][*nido*-6-CB<sub>9</sub>H<sub>12</sub>] (39 mg; 0.2 mmol) in CH<sub>2</sub>Cl<sub>2</sub>. Thus, though the reaction with the methanol was in a 100% yield, the total route gave 12% of the methoxy derivative based on [*cis*-PtCl<sub>2</sub>(PMe<sub>2</sub>Ph)<sub>2</sub>]. The mass spectrum of 2 gives an envelope with *m/z* (max.) at 623 amu corresponding to a molecular formula <sup>12</sup>C<sub>18</sub><sup>1</sup>H<sub>35</sub><sup>31</sup>P<sub>2</sub><sup>11</sup>B<sub>9</sub><sup>16</sup>O<sup>195</sup>Pt.

## Acknowledgements

Contribution no. 112 from the Leeds-Rez Anglo-Czech Polyhedral Collaboration (ACPC); we thank the Royal Society and the Academy of Sciences of the Czech Republic for support of the collaboration. We thank the EPSRC for contributions towards instrumentation and Dr Jane Jones for some initial work. We also

thank the Basque Government for a predoctoral Grant to RM, and the Spanish Ministry of Education for financial support under the "Ramón y Cajal Program". Computing work performed by JB was self-financed.

## References

- G. Ferguson, M. C. Jennings, A. J. Lough, S. Coughlan, T. R. Spalding, J. D. Kennedy, X. L. R. Fontaine and B. Štíbr, *J. Chem. Soc., Chem. Commun.*, 1990, 891–894.
- B. Štíbr, T. Jelínek, J. D. Kennedy, X. L. R. Fontaine and M. Thornton-Pett, *J. Chem. Soc., Dalton Trans.*, 1993, 1261–1267.
- R. E. Williams, *Adv. Inorg. Chem. Radiochem.*, 1976, **18**, 67–142; K. Wade, *Adv. Inorg. Chem. Radiochem.*, 1976, **18**, 1–66.
- R. Macías, N. P. Rath and L. Barton, *Organometallics*, 1999, **18**, 3637–3648; R. Macías, N. P. Rath and L. Barton, *Angew. Chem., Int. Ed.*, 1999, **38**, 162–164; O. Volkov, R. Macías, N. P. Rath and L. Barton, *Appl. Organomet. Chem.*, 2003, **17**, 409–420; O. Volkov, R. Macías, N. P. Rath and L. Barton, *Inorg. Chem.*, 2002, **41**, 5837–5843; M. Murphy, T. R. Spalding, G. Ferguson and J. F. Gallagher, *Acta Crystallogr., Sect. C: Cryst. Struct. Commun.*, 1992, **48**, 638–641; G. Ferguson, A. L. Lough, S. Coughlan and T. R. Spalding, *Acta Crystallogr., Sect. C: Cryst. Struct. Commun.*, 1992, **48**, 440–443; S. Coughlan, T. R. Spalding, G. Ferguson, J. F. Gallagher, A. J. Lough, X. L. R. Fontaine, J. D. Kennedy and B. Štíbr, *J. Chem. Soc., Dalton Trans.*, 1992, 2865–2871.
- L. Wesemann, in *Comprehensive Organometallic Chemistry III*, ed. D. M. P. Mingos and R. H. Crabtree, Elsevier, Oxford, 2007, vol. 3, p. 125.
- K. J. Adams, T. D. McGrath, G. M. Rosair, A. S. Weller and A. J. Welch, *J. Organomet. Chem.*, 1998, **550**, 315–329.
- M. P. Murphy, T. R. Spalding, C. Cowey, J. D. Kennedy, M. Thornton-Pett and J. Holub, *J. Organomet. Chem.*, 1998, **550**, 151–164; J. D. Kennedy, in *The Borane-Carborane-Carbocation Continuum*, ed. J. Casanova, Wiley, New York, 1998, pp. 85–116.
- B. Štíbr, T. Jelínek, J. Plešek and S. Heřmánek, *J. Chem. Soc., Chem. Commun.*, 1987, 963–964.
- R. W. Rudolph and W. R. Pretzer, *Inorg. Synth.*, 1983, **22**, 226–231.
- K. Baše, *Collect. Czech. Chem. Commun.*, 1983, **48**, 2593–2603.
- C. W. Jung and M. F. Hawthorne, *J. Am. Chem. Soc.*, 1980, **102**, 3024–3032.
- H. Fowkes, N. N. Greenwood, J. D. Kennedy and M. Thornton-Pett, *J. Chem. Soc., Dalton Trans.*, 1986, 517–523; D. A. Thompson, T. K. Hilty and R. W. Rudolph, *J. Am. Chem. Soc.*, 1977, **99**, 6774–6775; T. K. Hilty, D. A. Thompson, W. M. Butler and R. W. Rudolph, *Inorg. Chem.*, 1979, **18**, 2642–2651.
- J. D. Kennedy, in *Multinuclear NMR*, ed. J. Mason, Plenum, New York, 1987, pp. 221–224.
- J. D. Kennedy, I. J. Colquhoun, W. McFarlane and R. J. Puddephatt, *J. Organomet. Chem.*, 1979, **172**, 479–489.
- K. Nestor, X. L. R. Fontaine, J. D. Kennedy, B. Štíbr, K. Baše and M. Thornton-Pett, *Collect. Czech. Chem. Commun.*, 1991, **56**, 1607–1617.
- M. A. Beckett and J. D. Kennedy, *J. Chem. Soc., Chem. Commun.*, 1983, 575–576; M. Bown, X. L. R. Fontaine and J. D. Kennedy, *J. Chem. Soc., Dalton Trans.*, 1988, 1467–1473.
- S. Heřmánek, *Chem. Rev.*, 1992, **92**, 325–362.
- J. Bould, W. Clegg and J. D. Kennedy, *Inorg. Chim. Acta*, 2006, **359**, 3723–3735.
- O. Volkov, R. Macías, N. P. Rath and L. Barton, *J. Organomet. Chem.*, 2002, **657**, 40–47.
- K. Nestor, X. L. R. Fontaine, N. N. Greenwood, J. D. Kennedy, J. Plešek, B. Štíbr and M. Thornton-Pett, *Inorg. Chem.*, 1989, **28**, 2219–2221.
- D. A. Kleier, D. A. Dixon and W. N. Lipscomb, *Inorg. Chem.*, 1978, **17**, 166–167; E. G. Kononova, L. A. Leites, S. S. Bukalov, I. V. Pisareva, I. T. Chizhevsky, J. D. Kennedy and J. Bould, submitted to *Eur. J. Inorg. Chem.*.
- J. D. Kennedy, B. Štíbr, T. Jelínek, X. L. R. Fontaine and M. Thornton-Pett, *Collect. Czech. Chem. Commun.*, 1993, **58**, 2090–2120.
- G. Ferguson, M. Parvez, J. A. MacCurtain, O. N. Dhuhghaill, T. R. Spalding and D. Reed, *J. Chem. Soc., Dalton Trans.*, 1987, 699–704; Faridoo, O. N. Dhuhghaill, T. R. Spalding, G. Ferguson, B. Kaiter, X. L. R. Fontaine and J. D. Kennedy, *J. Chem. Soc., Dalton Trans.*, 1989,

- 1657–1668; G. Ferguson, J. D. Kennedy, X. L. R. Fontaine, Faridooon and T. R. Spalding, *J. Chem. Soc., Dalton Trans.*, 1988, 2555–2564; G. Ferguson, J. F. Gallagher, M. McGrath, J. P. Sheehan, T. R. Spalding and J. D. Kennedy, *J. Chem. Soc., Dalton Trans.*, 1993, 27–34; S. R. Bunkhall, X. L. R. Fontaine, N. N. Greenwood, J. D. Kennedy and M. Thornton-Pett, *J. Chem. Soc., Dalton Trans.*, 1990, 73–79; M. McGrath, T. R. Spalding, X. L. R. Fontaine, J. D. Kennedy and M. Thornton-Pett, *J. Chem. Soc., Dalton Trans.*, 1991, 3223–3233; D. Oconnell, J. C. Patterson, T. R. Spalding, G. Ferguson, J. F. Gallagher, Y. W. Li, J. D. Kennedy, R. Macías, M. Thornton-Pett and J. Holub, *J. Chem. Soc., Dalton Trans.*, 1996, 3323–3333.
- 24 K. Baše, B. Štíbr, J. Dolanský and J. Duben, *Collect. Czech. Chem. Commun.*, 1981, **46**, 2345–2353.
- 25 J. M. Jenkins and B. L. Shaw, *J. Chem. Soc. A*, 1966, 770–775; J. A. Osborn and G. Wilkinson, *Inorg. Synth.*, 1967, **10**, 67–71.
- 26 J. D. Kennedy, X. L. R. Fontaine, M. McGrath and T. R. Spalding, *Magn. Reson. Chem.*, 1991, **29**, 711; M. Bown, X. L. R. Fontaine, N. N. Greenwood and J. D. Kennedy, *Z. Anorg. Allg. Chem.*, 1991, **602**, 17–29.
- 27 D. Reed, *Chem. Soc. Rev.*, 1993, 109–116.
- 28 J. D. Kennedy, W. McFarlane, R. J. Puddephatt and P. J. Thompson, *J. Chem. Soc., Dalton Trans.*, 1976, 874–879.
- 29 U. Meier, C. van Wüllen and M. Schindler, *J. Comput. Chem.*, 1992, **13**, 551; W. Kutzelnigg, M. Schindler and U. Fleischer, in *NMR, Basic Principles and Progress*, Springer Verlag, Berlin, New York, 1990, p. 165; M. J. Frisch, G. W. Trucks, H. B. Schlegel, G. E. Scuseria, M. A. Robb, J. R. Cheeseman, V. G. Zakrzewski, J. A. Montgomery, Jr., R. E. Stratmann, J. C. Burant, S. Dapprich, J. M. Millam, A. D. Daniels, K. N. Kudin, M. C. Strain, O. Farkas, J. Tomasi, V. Barone, M. Cossi, R. Cammi, B. Mennucci, C. Pomelli, C. Adamo, S. Clifford, J. Ochterski, G. A. Petersson, P. Y. Ayala, Q. Cui, K. Morokuma, D. K. Malick, A. D. Rabuck, K. Raghavachari, J. B. Foresman, J. Cioslowski, J. V. Ortiz, A. G. Baboul, B. B. Stefanov, G. Liu, A. Liashenko, P. Piskorz, I. Komaromi, R. Gomperts, R. L. Martin, D. J. Fox, T. Keith, M. A. Al-Laham, C. Y. Peng, A. Nanayakkara, C. Gonzalez, M. Challacombe, P. M. W. Gill, B. G. Johnson, W. Chen, M. W. Wong, J. L. Andres, M. Head-Gordon, E. S. Replogle and J. A. Pople, *GAUSSIAN 98 (Revision A.7)*, Gaussian, Inc., Pittsburgh, PA, 1998; M. J. Frisch, G. W. Trucks, H. B. Schlegel, G. E. Scuseria, M. A. Robb, J. R. Cheeseman, J. A. Montgomery, Jr., T. Vreven, K. N. Kudin, J. C. Burant, J. M. Millam, S. S. Iyengar, J. Tomasi, V. Barone, B. Mennucci, M. Cossi, G. Scalmani, N. Rega, G. A. Petersson, H. Nakatsuji, M. Hada, M. Ehara, K. Toyota, R. Fukuda, J. Hasegawa, M. Ishida, T. Nakajima, Y. Honda, O. Kitao, H. Nakai, M. Klene, X. Li, J. E. Knox, H. P. Hratchian, J. B. Cross, V. Bakken, C. Adamo, J. Jaramillo, R. Gomperts, R. E. Stratmann, O. Yazyev, A. J. Austin, R. Cammi, C. Pomelli, J. Ochterski, P. Y. Ayala, K. Morokuma, G. A. Voth, P. Salvador, J. J. Dannenberg, V. G. Zakrzewski, S. Dapprich, A. D. Daniels, M. C. Strain, O. Farkas, D. K. Malick, A. D. Rabuck, K. Raghavachari, J. B. Foresman, J. V. Ortiz, Q. Cui, A. G. Baboul, S. Clifford, J. Cioslowski, B. B. Stefanov, G. Liu, A. Liashenko, P. Piskorz, I. Komaromi, R. L. Martin, D. J. Fox, T. Keith, M. A. Al-Laham, C. Y. Peng, A. Nanayakkara, M. Challacombe, P. M. W. Gill, B. G. Johnson, W. Chen, M. W. Wong, C. Gonzalez and J. A. Pople, *GAUSSIAN 03 (Revision B.05)*, Gaussian, Inc., Wallingford, CT, 2004.
- 30 J. Bould, T. Jelinek, S. A. Barrett, S. J. Coles, M. J. Hursthouse, M. Thornton-Pett, B. Štíbr and J. D. Kennedy, *Dalton Trans.*, 2005, 1449–1503.
- 31 P. Y. Ayla and H. B. Schegel, *J. Chem. Phys.*, 1997, **107**, 375.